

## McCARD/G TRANSIENT ANALYSIS FOR CABRI-LIKE BENCHMARK

Jae Young Kwon and Hyung Jin Shim\*

Department of Nuclear Engineering, Seoul National University, 1 Gwanak-ro, Gwanak-gu,  
Seoul 08826, Republic of Korea

\*shimhj@snu.ac.kr

\*Keywords : CABRI-like benchmark, transient analysis, time-dependent Monte Carlo, McCARD/G

### 1. Introduction

Transient analysis is essential for examining the dynamic characteristics of a reactor when it deviates from its normal state and undergoes time-dependent changes. This analysis is crucial for reactor safety evaluation and design optimization, playing a key role in accurately predicting core behavior under abnormal or accident conditions. However, transient analysis requires performing core calculations over thousands of time steps, demanding excessive computational resources. Monte Carlo methods, in particular, have faced significant challenges in making transient analysis feasible due to their intensive computational requirements.

Recent advancements have led to the development of efficient and high-accuracy methodologies for the time-dependent Monte Carlo (TDMC) neutron transport calculation [1-3], making reactor transient analysis feasible within a practical time range. The developed methodologies have been implemented in the GPU-accelerated version of McCARD [4], McCARD/G [5].

This study aims to verify the transient analysis capability of McCARD/G by performing a transient analysis of the CABRI-like benchmark using TDMC calculations. CABRI is an experimental reactor built in France by the French Alternative Energies and Atomic Energy Commission (CEA) in the 1960s. Dynamic reactivity, temperature, and power are evaluated over a short time period (0.2 seconds) following the depressurization of the He-3 rod, which serves as a neutron absorber. The calculated results are compared with those obtained by the point kinetics equation (PKE).

### 2. Modeling for the CABRI-Like Benchmark

The CABRI-like benchmark [6] has been analyzed by the McCARD/G. Figures 1-3 show its geometrical models generated using McView [7] for McCARD and McCARD/G.

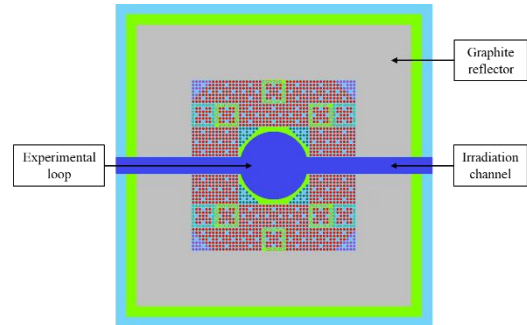


Figure 1. Horizontal cross section of the McCARD/G model for the CABRI-like benchmark

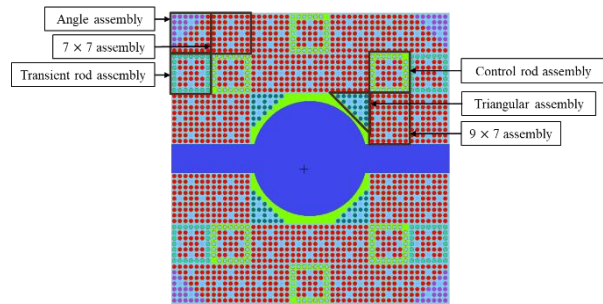


Figure 2. Horizontal cross section of the McCARD/G core model for the CABRI-like benchmark

#### 2.1. Transient scenario for the CABRI-like benchmark

This study analyzes three transient scenarios classified as LOW, INTER, and HIGH. Each scenario is defined by the following characteristics [6]:

**LOW scenario:** The transient should not be prompt critical, as the insertion of reactivity is below  $\beta_{\text{eff}}$ .

**INTER scenario:** The transient be prompt critical, as the insertion of reactivity is approximately  $\beta_{\text{eff}}$ .

**HIGH scenario:** The transient is sharp and violent, with the insertion of reactivity significantly exceeding  $\beta_{\text{eff}}$ .

In the scenarios, the reactivity is inserted through the extraction of He-3 from the helium tubes in the transient rod assembly, shown in Figure 3. In the benchmark, the helium tube is assumed to be initially filled with the pure He-3. Table 1 presents the initial and minimum He-3 densities for the three transient scenarios.

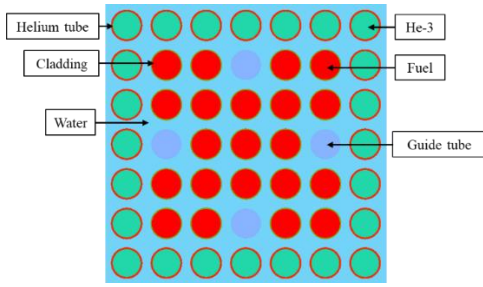


Figure 3. Horizontal cross section of the transient rod assembly

Table 1. The initial and minimum He-3 densities in transient scenarios

Scenario	Initial He-3 density [atoms/barn·cm]	Min. He-3 density [atoms/barn·cm]
LOW	$1.775 \times 10^5$	$1.353 \times 10^6$
INTER	$6.321 \times 10^5$	$3.667 \times 10^6$
HIGH	$2.796 \times 10^4$	$1.592 \times 10^5$

## 2.2. Transient scenario for the CABRI-Like benchmark

In the McCARD/G transient analysis, temperature feedback is incorporated by updating the temperatures of 11,904 fuel cells at each time step. Each of the 1,488 fuel rods is axially divided into eight cells. The temperature of the  $n$ -th fuel cell in time step  $i$ , denoted by  $T_n^i$ , is updated by [8]

$$T_n^i = T_n^{i-1} + \frac{Q_n^{i-1} - Q_n^{i=0}}{m_n c_p}, \quad (1)$$

where  $Q_n^i$  represents the energy accumulated in the fuel cell  $n$  during time step  $i$ .  $m$  is the mass of  $\text{UO}_2$  (in kg) and  $c_p$  is 300 J/kg·K, [8].

## 3. Eigenvalue Calculations

Prior to calculating the transient scenarios, reactivity worth by the He-3 extraction for each scenario is calculated by the McCARD/G eigenvalue calculations. The McCARD/G eigenvalue calculations are performed on 500,000 histories per cycle for 200 inactive and 1,000 active cycles with the ENDF/B-VII.1 libraries [9].

Table 2 and 3 show comparisons of  $k_{\text{eff}}$  at the initial state and inserted reactivities of each transient scenario calculated by McCARD/G with references [6], estimated using TRIPOLI and the JEFF3.1.1 libraries. In the table, SD means the standard deviation. The results indicate that the  $k_{\text{eff}}$  values estimated by McCARD/G are slightly higher than the reference values exceeding their 99% statistical confidence intervals. However, the inserted reactivities agree well within their 95% statistical confidence intervals.

Table 2. Results of  $k_{\text{eff}}$  in the initial steady-state

scenario	$k_{\text{eff}}$ in the initial steady-state (SD)		Diff. [pcm] (SD)
	McCARD/G	Reference	
LOW	1.0035 (0.00004)	0.99929 (0.0002)	106 (20)
INTER	1.00094 (0.00004)	0.99974 (0.0002)	120 (20)
HIGH	1.00128 (0.00004)	0.99943 (0.0002)	85 (20)

Table 3. Results of inserted reactivity

scenario	Inserted reactivity [pcm] (SD)		Diff. [pcm] (SD)
	McCARD/G	Reference	
LOW	599 (4)	581 (20)	18 (20)
INTER	1493 (4)	1489 (20)	4 (20)
HIGH	2635 (4)	2623 (20)	12 (20)

## 4. Modelling for Point Kinetics Analysis

In this study, the McCARD/G transient analysis results are compared with those obtained from a point kinetics equation (PKE) model. Taking into account the reactivity changes due to He-3 extraction and temperature feedback, the PKE model can be written as

$$\frac{dn(t)}{dt} = \frac{(\rho_{\text{He}}(t) + \rho_T(t) - \beta_{\text{eff}})}{\Lambda} n(t) - \sum_{i=1}^6 \lambda_i C_i(t), \quad (2)$$

$$\frac{dC_i}{dt} = \frac{\beta_{\text{eff},i}}{\Lambda} n(t) - \lambda_i C_i(t), \quad (3)$$

where  $\rho_{\text{He}}(t)$  and  $\rho_T(t)$  denote the reactivity changes due to the He-3 depressurization and the fuel temperature change, respectively.  $n(t)$  is the neutron density and the other notations follows the standard. In the PKE analysis, the kinetic parameters were obtained from the McCARD calculation results.

### 4.1. Reactivity change estimation due to He-3 depressurization

For the PKE analysis, the reactivity changes due to the He-3 depressurization, denoted as  $\rho_{\text{He}}(t)$ , should be calculated for the three transient scenarios: LOW, INTER, and HIGH. The first step in calculating  $\rho_{\text{He}}(t)$  for each transient scenario is to estimate the reactivity change according to the He-3 density. To accomplish this, a total of nine calculations, including the initial steady-state eigenvalue calculation, are conducted. These calculations are performed by varying the He-3 density at intervals corresponding to each 0.01-second step, beginning from the onset of He-3 extraction and continuing up to 0.08 seconds, during which the He-3 density rapidly decreases. The inserted reactivity

depending on He-3 density for each scenario is determined through interpolation. Then,  $\rho_{He}(t)$  for each transient scenario can be obtained using the He-3 density change provided in the benchmark [6]. Figure 4-6 show  $\rho_{He}(t)$  for the three transient scenarios.

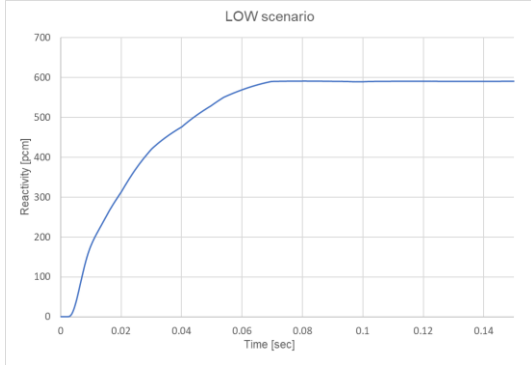


Figure 4. Reactivity inserted due to He-3 over time for LOW scenario

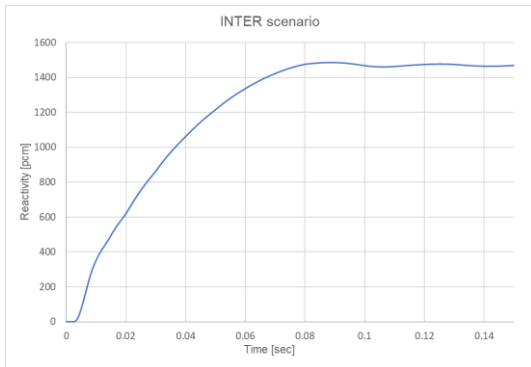


Figure 5. Reactivity inserted due to He-3 over time for INTER scenario

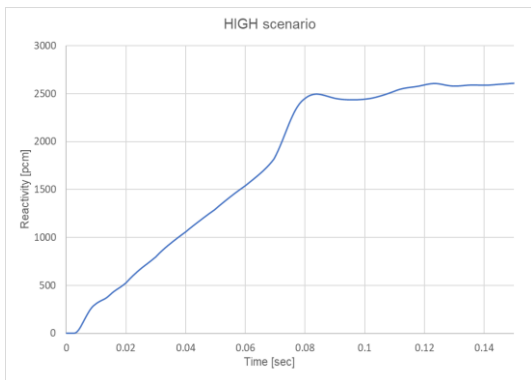


Figure 6. Reactivity inserted due to He-3 over time for HIGH scenario

#### 4.2. Modeling of Reactivity Change Due to Fuel Temperature Change

For the treatment of  $\rho_T(t)$  in the PKE analysis, the reactivity change according to the fuel temperature is estimated by the McCARD/G eigenvalue calculations with changing average fuel temperature. Figure 7 shows

the average fuel temperature dependent reactivity changes calculated by McCARD/G.

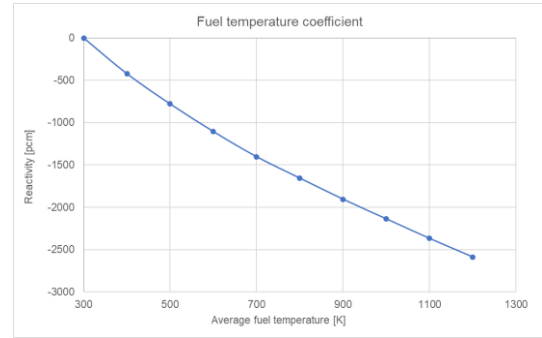


Figure 7. Reactivity loss due to temperature increase

Then, in the PKE analysis,  $\rho_T$  at time step  $i$  is calculated by Figure 7 corresponding to the fuel temperature estimated by

$$\frac{dT(t)}{dt} = \frac{P \cdot (n(t) - n_0)}{mc_p}, \quad (4)$$

where  $T(t)$  is the temperature, and  $P$  is the reactor power,  $n_0$  is the initial neutron density. The initial temperature and reactor power are set to 300K and 0.1 MW, respectively.

## 5. Numerical Results

The time-dependent behavior of dynamic reactivity, total power, and average fuel temperature for the three transient scenarios is evaluated by the McCARD/G time-dependent (TD) calculations and the PKE analysis. The McCARD/G TD calculations are performed by 2,000,000 histories per time interval, of which size is 0.0001 seconds, with 100 neutron convergence and 500 delayed neutron convergence steps, using the continuous cross section libraries from ENDF/B-VII.1. The results calculated by McCARD/G TD are provided with  $1\sigma$  error bars. The PKE calculation is performed using MATLAB, with a time step of 0.0001 seconds.

### 5.1. Results for the LOW scenario

Figure 8 shows a comparison of dynamic reactivities and Figure 9 shows the total power and average fuel temperature calculated by McCARD/G TD and PKE for the LOW scenario.

In both calculations, the dynamic reactivity increases over time and converges at approximately 600 pcm. Before 0.08 seconds, the dynamic reactivities from McCARD/G TD are slightly higher than those from the PKE exceeding their 95% statistical confidence intervals. However, after 0.08 seconds, the dynamic reactivities from McCARD/G TD are slightly lower than those from the PKE exceeding their 95% statistical confidence intervals.

Throughout the entire transient time range, the power results obtained from the PKE are generally higher than those obtained from McCARD/G TD. A comparison of the maximum power reveals a difference of 2.5% between the two calculations. The temperature values obtained from the PKE remain consistently higher than those obtained from McCARD/G TD across the entire transient period. The maximum temperature shows a difference of 0.01 K between the two calculations

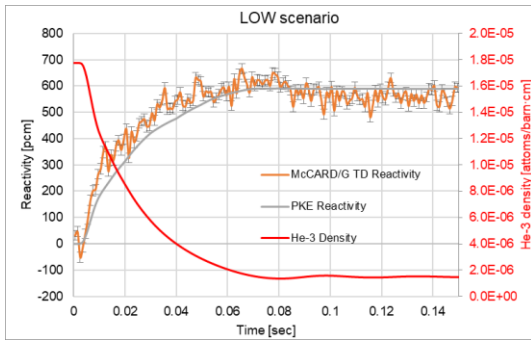


Figure 8. Dynamic reactivity He-3 density over time for the LOW scenario

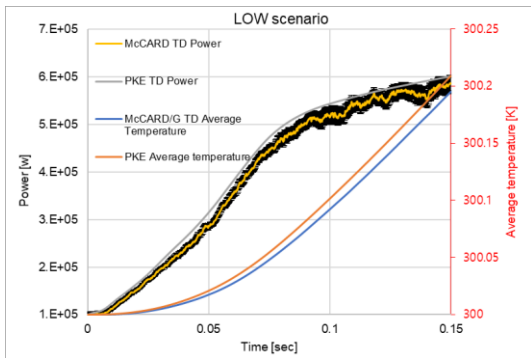


Figure 9. Power and average temperature over time for the LOW scenario

### 5.2. Results for the INTER scenario

Figure 10 presents a comparison of dynamic reactivities and Figure 11 presents the total power and the average fuel temperature calculated by McCARD/G TD and the PKE for the INTER scenario.

In the McCARD/G TD calculation, the dynamic reactivity initially increases by approximately 2200 pcm, then decreases to around -800 pcm, and subsequently rises again to converge at around 50 pcm over time. However, in the PKE calculation, the dynamic reactivity increases to approximately 1350 pcm, then decreases and converges at around 80 pcm.

Unlike the LOW scenario, which exhibited only minor differences in dynamic reactivity between McCARD/G TD and PKE, the INTER scenario presents a significant maximum deviation exceeding 800 pcm. This discrepancy is likely attributed to variations in the neutron spectrum and power distribution between the three-dimensional TD simulations of McCARD/G and

the steady-state-based PKE analysis. While similar differences also occur in the LOW scenario, their magnitude is relatively small and not as noticeable.

Regarding power, the results calculated by McCARD/G TD and the PKE are generally consistent throughout the entire transient time range within the 95% statistical confidence intervals. When comparing the maximum power, a difference of 12.9% is found. However, the temperature values calculated by the PKE are observed to be lower than those calculated by McCARD/G TD after 0.08 seconds throughout the transient period. The maximum temperature difference between the two calculations is found to be 54 K

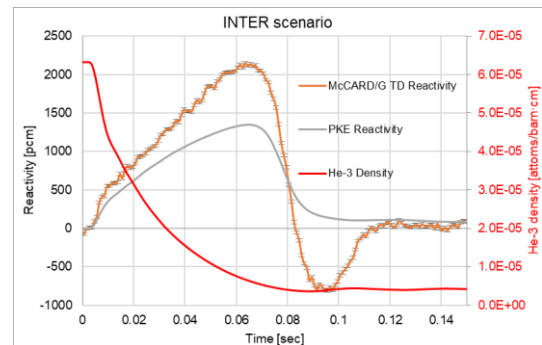


Figure 10. Dynamic reactivity and He-3 density over time for the INTER scenario

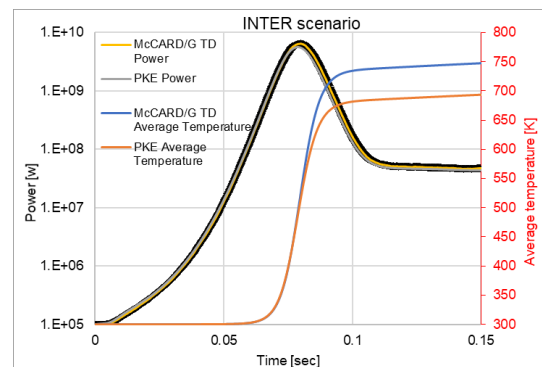


Figure 11. Power and average temperature over time for the INTER scenario

### 5.3. Results for the HIGH scenario

Figure 12 presents a comparison of dynamic reactivities and Figure 13 presents the total power and the average fuel temperature calculated by McCARD/G TD and the PKE for the HIGH scenario.

In the McCARD/G TD calculation, the dynamic reactivity initially rises to approximately 2700 pcm, then decreases to around -1500 pcm, and subsequently rises again to converge at approximately -100 pcm over time. However, in the PKE calculation, the dynamic reactivity rises to 1590 pcm, then decreases and converges at around -20 pcm. Similar to the INTER scenario, this discrepancy may arise due to the point kinetics assumptions including the kinetics parameters calculated in the steady-state condition.

The power results are generally consistent throughout the entire transient time range within the 95% statistical confidence interval. A comparison of the maximum power reveals a 4.9% difference between the two calculations. However, after 0.07 seconds, the temperature values calculated by the PKE are lower than those calculated by McCARD/G TD for the remainder of the transient period. The maximum temperature difference between the two calculations is found to be 88 K

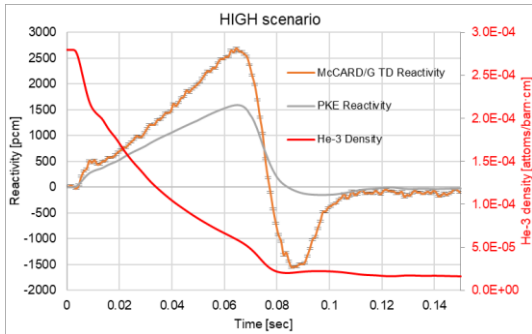


Figure 12. Dynamic reactivity and He-3 density over time for the HIGH scenario

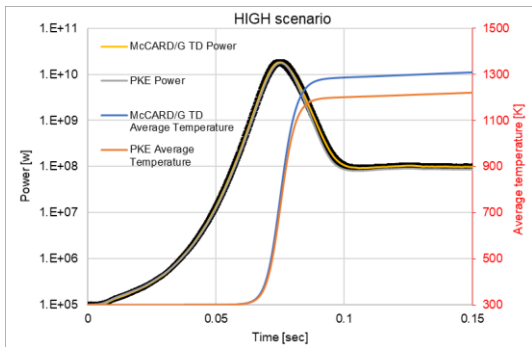


Figure 13. Power and average temperature over time for the HIGH scenario

### 6. Analysis for Assembly-Level T/H Feedback

Additionally, the McCARD/G TD calculations are performed with assembly-level T/H feedback with and without axial segmentation into 10 sections fine cell instead of fine cell T/H feedback. Figure 14 shows assembly regions with applied T/H feedback.

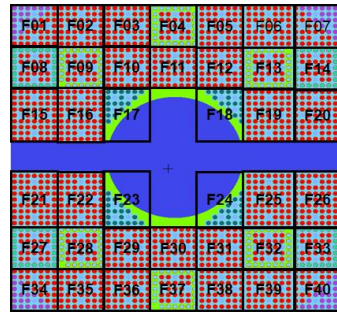
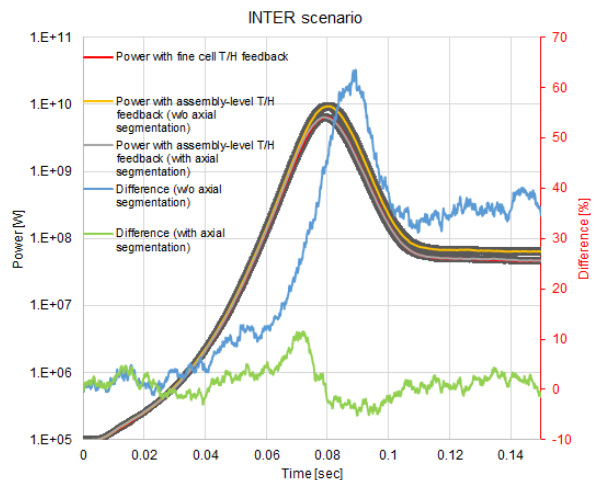


Figure 14. Assembly regions with applied T/H feedback

The power and temperature results for the INTER and HIGH scenarios are compared based on the method of fine cell T/H feedback application and assembly-level T/H feedback application. For the case of difference, both the assembly-level T/H feedback with axial segmentation and the one without segmentation are compared with the fine cell T/H feedback.

Figure 15 and 16 show the power and average temperature over time for the INTER and HIGH scenario, respectively. For power, in the INTER scenario, when compared with the fine cell T/H feedback, the case with axial segmentation has a maximum difference of about 10%, while the case without axial segmentation has a difference of up to 60%. In the HIGH scenario, the case with axial segmentation has a difference of about 30%, while the case without axial segmentation has a difference of about 70%. For temperature, in the INTER scenario, the difference is 8 K with axial segmentation and 196 K without it. In the HIGH scenario, the difference is 66 K with axial segmentation and 443 K without it.

This demonstrates that, when applying T/H feedback in core transient analysis, there is a significantly larger difference in both power and temperature when axial segmentation for T/H feedback is used, compared to when it is not, confirming the importance of T/H feedback with axial segmentation.



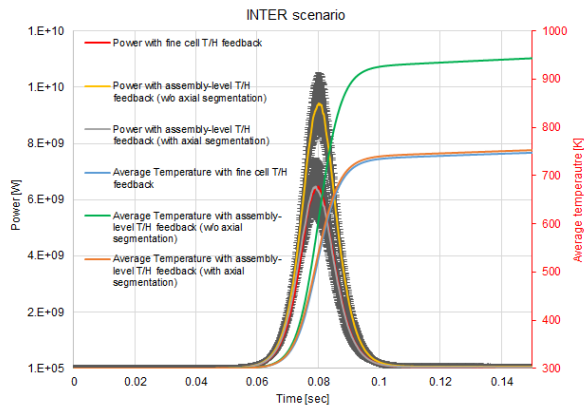


Figure 15. Power and average temperature over time for the INTER scenario

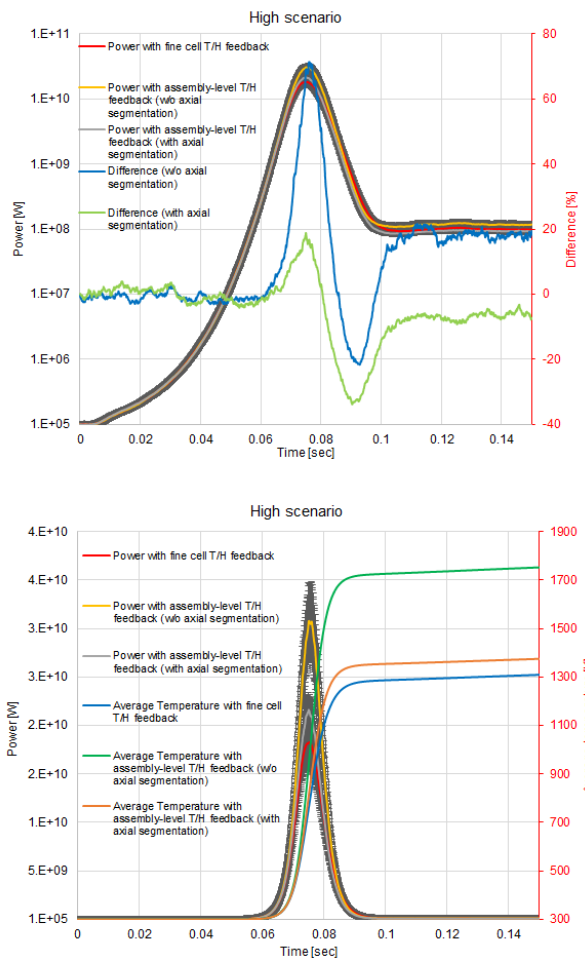


Figure 16. Power and average temperature over time for the HIGH scenario

### 7. Conclusion

This study analyzed the LOW, INTER, and HIGH scenarios using McCARD/G TD and the PKE. The analysis revealed noticeable differences in dynamic reactivities between the two methods which can arise due to the point kinetics assumptions. In contrast, power

results from the both methods are found to be consistent within the 95% statistical confidence interval across all the three scenarios. For the maximum power, differences of -2.5%, 12.9%, and 4.9% are observed for the LOW, INTER, and HIGH scenarios, respectively. Additionally, differences in temperature values between the two calculations are identified. For the maximum temperature, differences of 0.01 K, 54 K, and 88.19 K are observed between the two calculations for the respective scenarios. Additionally, the McCARD/G TD calculations are performed with assembly-level T/H feedback with and without axial segmentation into 10 sections. The results reveal a significantly larger difference in both power and temperature when axial segmentation for T/H feedback is used, compared to when it is not, confirming the critical importance of axial segmentation in core transient analysis.

### REFERENCES

- [1] Cullen, D. E., Clouse, C. J., Procassini, R., & Little, R. C. (2003). *Static and dynamic criticality: are they different?* (No. UCRL-TR-201506). Lawrence Livermore National Lab.(LLNL), Livermore, CA (United States).
- [2] Legrady, D., & Hoogenboom, J. E. (2008). Scouting the feasibility of Monte Carlo reactor dynamics simulations.
- [3] Sjenitzer, B. L., & Hoogenboom, J. E. (2013). Dynamic Monte Carlo method for nuclear reactor kinetics calculations. *Nuclear Science and Engineering*, 175(1), 94-107.
- [4] Shim, H. J., Han, B. S., Jung, J. S., Park, H. J., & Kim, C. H. (2012). McCARD: Monte Carlo code for advanced reactor design and analysis. *Nuclear Engineering and Technology*, 44(2), 161-176.
- [5] Ko, W. K., Jeong, S. J., Kim, Y. I., & Shim, H. J. (2024). Development of a GPU-enhanced time-dependent Monte Carlo neutron transport version of McCARD. *EPJ Nuclear Sciences & Technologies*, 10, 28.
- [6] Jaboulay, J. C., and Jaboulay, J. (2024). CABRI-based benchmark: Geometrical description and material balance. version 2.
- [7] Jeong, S. J., & Shim, H. J. (2022, October). McView: McCARD Input Visualization Tool. In Transactions of the Korean Nuclear Society Autumn Meeting, Changwon, Korea.
- [8] Ferraro, D. and Ferrari, I. (2024, October). INVAP's first results for CABR numerical problem, IAEA CRP F12028.
- [9] Chadwick, M. B., Herman, M., Obložinský, P., Dunn, M. E., Danon, Y., Kahler, A. C., ... & Young, P. G. (2011). ENDF/B-VII. 1 nuclear data for science and technology: cross sections, covariances, fission product yields and decay data. *Nuclear data sheets*, 112(12), 2887-2996.